

## INSPIRALLING SUPERMASSIVE BLACK HOLES: A NEW SIGNPOST FOR GALAXY MERGERS

JULIA M. COMERFORD<sup>1</sup>, BRIAN F. GERKE<sup>2</sup>, JEFFREY A. NEWMAN<sup>3</sup>, MARC DAVIS<sup>1,4</sup>, RENBIN YAN<sup>5</sup>, MICHAEL C. COOPER<sup>6,7</sup>,  
S.M. FABER<sup>8</sup>, DAVID C. KOO<sup>8</sup>, ALISON L. COIL<sup>6,9,10</sup>, D.J. ROSARIO<sup>8</sup>, AND AARON A. DUTTON<sup>8</sup>

<sup>1</sup>Astronomy Department, 601 Campbell Hall, University of California, Berkeley, CA 94720

<sup>2</sup>Kavli Institute for Particle Astrophysics and Cosmology, M/S 29, Stanford Linear Accelerator Center,  
2575 Sand Hill Rd., Menlo Park, CA 94725

<sup>3</sup>Department of Physics and Astronomy, University of Pittsburgh, Pittsburgh, PA 15260

<sup>4</sup>Department of Physics, University of California, Berkeley, CA 94720

<sup>5</sup>Department of Astronomy and Astrophysics, University of Toronto, Toronto, ON M5S3H8, Canada

<sup>6</sup>Steward Observatory, University of Arizona, Tucson, AZ 85721

<sup>7</sup>Spitzer fellow

<sup>8</sup>UCO/Lick Observatory, Department of Astronomy and Astrophysics, University of California, Santa Cruz, CA 95064

<sup>9</sup>Hubble fellow and

<sup>10</sup>Department of Physics, University of California, San Diego, CA 92093

*Draft version December 4, 2018*

### ABSTRACT

We present a new technique for observationally identifying galaxy mergers spectroscopically rather than through host galaxy imaging. Our technique exploits the dynamics of supermassive black holes (SMBHs) powering active galactic nuclei (AGNs) in merger-remnant galaxies. Because structure in the universe is built up through galaxy mergers and nearly all galaxies host a central SMBH, some galaxies should possess two SMBHs near their centers as the result of a recent merger. These SMBHs spiral to the center of the resultant merger-remnant galaxy, and one or both of the SMBHs may power AGNs. Using the DEEP2 Galaxy Redshift Survey, we have examined 1881 red galaxies, of which 91 exhibit [O III] and H $\beta$  emission lines indicative of Seyfert 2 activity. Of these, 32 AGNs have [O III] emission-line redshifts significantly different from the redshifts of the host galaxies' stars, corresponding to velocity offsets of  $\sim 50$  km s<sup>-1</sup> to  $\sim 300$  km s<sup>-1</sup>. Two of these AGNs exhibit double-peaked [O III] emission lines, while the remaining 30 AGNs each exhibit a single set of velocity-offset [O III] emission lines. After exploring a variety of physical models for these velocity offsets, we argue that the most likely explanation is inspiralling SMBHs in merger-remnant galaxies. Based on this interpretation, we find that roughly half of the red galaxies hosting AGNs are also merger remnants, which implies that mergers may trigger AGN activity in red galaxies. The AGN velocity offsets we find imply a merger fraction of  $\sim 30\%$  and a merger rate of  $\sim 3$  mergers Gyr<sup>-1</sup> for red galaxies at redshifts  $0.34 < z < 0.82$ .

*Subject headings:* galaxies: active – galaxies: interactions – galaxies: nuclei – galaxies: Seyfert

### 1. INTRODUCTION

In the current  $\Lambda$  cold dark matter cosmological paradigm, galaxies grow hierarchically through mergers that combine smaller galaxies to build a more massive remnant galaxy. The massive, early-type galaxies observed in the local universe appear to have largely been built up by such processes from  $z \sim 1$  to the present. The amount of mass in stars in early-type galaxies has been observed to increase as the universe evolves to the present time (e.g., Bundy et al. 2005), which implies that other galaxies are transforming into early-type galaxies (since they are not forming stars themselves), and this buildup is believed to be connected to galaxy mergers (e.g., Hopkins et al. 2007). Galaxy mergers are thought to be instrumental not only in the evolution of late-type to early-type galaxies (Toomre & Toomre 1972), but also in initiating star formation, triggering inflows of gas, and initiating galaxy winds that can clear a galaxy of its gas (Springel et al. 2005b).

Central supermassive black holes (SMBHs) of a million to a billion solar masses are found in nearly all galaxies (Kormendy & Richstone 1995), and hierarchical structure formation thus implies that some galaxies should harbor two SMBHs near their centers as the result of a recent merger. If sufficient gas is available for accretion

onto a SMBH one or both of the SMBHs may power active galactic nuclei (AGNs).

Semianalytic models and numerical simulations show that AGN feedback quenches star formation and helps transform late-type galaxies into early-type galaxies (Springel et al. 2005a; Croton et al. 2006), which implies that we must understand how AGN activity is initiated in order to understand galaxy evolution. Galaxy mergers are in fact thought to play a role in funneling gas onto galaxy centers and fueling AGNs, as seen in numerical simulations (Springel et al. 2005a). Determining the fraction of AGNs that are found in galaxy mergers can help us calibrate the strength of this link.

The frequency of galaxy mergers is also central to our understanding of galaxy evolution, but the galaxy merger rate has proven difficult to measure observationally. The merger rate is usually estimated either from the number of close dynamical pairs of galaxies (typically defined as galaxies with separations less than 10 – 40 kpc and radial velocity differences below 500 km s<sup>-1</sup>) or the number of galaxies with morphological signatures of mergers such as tidal features and asymmetries (identified through visual inspection of galaxy images or quantitative methods). However, simulations of cosmic structure formation suggest that close pairs may not be good proxies for mergers

(Wetzel et al. 2008) and that merger timescales are typically underestimated (Kitzbichler & White 2008), while morphological merger identification often misclassifies galaxies (De Propris et al. 2007; Lotz et al. 2008).

In this paper, we present a new method of identifying galaxy mergers that is based on inspiralling SMBHs. Unlike other techniques for identifying galaxy mergers, our method relies on spectroscopy rather than host galaxy imaging. Further, our method involves a very different set of assumptions than those used in close pair counts or galaxy morphologies. The complete physical picture of our method is summarized below.

After a merger between two galaxies hosting central SMBHs, dynamical friction will cause the two SMBHs to inspiral toward the center of the merger-remnant galaxy. The two SMBHs will remain at separations  $\gtrsim 1$  kpc for  $\sim 100$  Myr, then form a SMBH binary of parsec-scale separation (Milosavljević & Merritt 2001; Begelman et al. 1980). Then, the SMBH binary must coalesce into a single central SMBH in the merger remnant in order to maintain the close observational correlation between black hole mass and velocity dispersion, or total mass, of the host galaxy’s stellar bulge (Ferrarese & Merritt 2000).

If sufficient gas is available, one or both of the SMBHs may power AGNs. AGN structure includes a very compact broad-line region (BLR;  $\sim 1$  pc in size) in the central part of the AGN and a more extended narrow-line region (NLR;  $\sim 100$  pc in size). If both SMBHs power AGNs, they could be visible as two independent AGN nuclei during the  $\sim 100$  Myr phase of the merger when their NLRs are not overlapping. In this case the merger-remnant galaxy spectrum would exhibit two sets of AGN emission lines, including the strong [O III] emission lines that are a signature of AGN activity. Both sets of emission lines would be separated both spatially and in velocity from each other and the host galaxy’s stellar continuum light. An example of this type of galaxy is EGSD2 J142033.6+525917, an early-type galaxy at  $z = 0.71$  with two sets of Seyfert 2 [O III] lines separated by  $630 \text{ km s}^{-1}$  and  $0.84 h^{-1}$  kpc (Gerke et al. 2007). We call such galaxies with two spatially resolved sets of [O III] emission lines “dual AGNs”.

If only one of the inspiralling SMBHs powers an AGN, then the merger-remnant galaxy spectrum would display one set of AGN emission lines that is separated both spatially and in velocity from the host galaxy’s stellar continuum light. An example of this type of galaxy is NGC 3341, a disturbed disk galaxy at  $z = 0.0271$  with a triple nucleus, where one nucleus is a confirmed Seyfert 2 with a blueshifted velocity of  $190 \text{ km s}^{-1}$  and a spatial offset of  $5.1$  kpc relative to the primary galaxy (Barth et al. 2008). We call such galaxies with one set of velocity-offset [O III] emission lines “offset AGNs”.

Because they are the result of inspiralling SMBHs during a galaxy merger, offset and dual AGNs are a powerful observational tool for identifying galaxy mergers. Offset and dual AGNs are expected to exhibit velocity shifts of up to a few hundred  $\text{km s}^{-1}$ , and the spatial separations are expected to be  $\sim 1$  kpc.

While there have been a few serendipitous discoveries of offset and dual AGNs, in this paper we conduct the first systematic survey of offset and dual AGNs. We identify 32 such Seyfert 2 galaxies – 30 offset AGNs and

two dual AGNs – in the DEEP2 Galaxy Redshift Survey, and use them to determine both the fraction of AGNs hosted by red galaxy mergers and the red galaxy merger rate. We assume a Hubble constant  $H_0 = 100 h \text{ km s}^{-1} \text{ Mpc}^{-1}$ ,  $\Omega_m = 0.3$ , and  $\Omega_\Lambda = 0.7$  throughout.

## 2. OBSERVATIONS AND ANALYSIS

The recently completed DEEP2 Galaxy Redshift Survey gives the most detailed view of the  $z \sim 1$  universe currently available. The survey covers  $\sim 3 \text{ deg}^2$  of sky, split over four separate fields, down to a limiting magnitude of  $R_{AB} = 24.1$ . Using the DEIMOS spectrograph on the Keck II telescope, DEEP2 obtained spectra for  $\sim 50,000$  galaxies out to  $z = 1.4$ . We consider a sample of 33,211 galaxies that have accurate redshift measurements (quality  $Q = 3$  or 4; see Davis et al. 2007).

### 2.1. Sample Selection

We first define a subset of galaxies hosting AGNs from the initial sample of 33,211 DEEP2 galaxies. AGN activity can be identified by a host galaxy’s location on the Baldwin-Phillips-Terlevich (BPT) diagram of line ratios, which is commonly used to identify the source of line emission in a galaxy (Baldwin et al. 1981; Kewley et al. 2006). High [O III]  $\lambda 5007/\text{H}\beta$  line flux ratios can indicate either AGN activity or star formation, and the BPT diagram uses [N II]  $\lambda 6583/\text{H}\alpha$  line flux ratios to distinguish between the two. High [O III]  $\lambda 5007/\text{H}\beta$  and high [N II]  $\lambda 6583/\text{H}\alpha$  signifies AGN activity, while high [O III]  $\lambda 5007/\text{H}\beta$  and low [N II]  $\lambda 6583/\text{H}\alpha$  signifies star formation. Because the limited wavelength coverage of DEEP2 (6500 – 9500 Å) prevents [N II]  $\lambda 6583$  and  $\text{H}\alpha$  from being covered in the same spectrum as [O III]  $\lambda 5007$  and  $\text{H}\beta$ , we instead use galaxy color to distinguish high [O III]  $\lambda 5007/\text{H}\beta$  AGN activity from high [O III]  $\lambda 5007/\text{H}\beta$  star formation. To accomplish this, we limit ourselves to galaxies on the red sequence, which necessarily also excludes AGNs that reside in blue galaxies.

To measure the flux of emission lines, we first fit a continuum spectrum to each galaxy spectrum. We mask out all emission lines present in each galaxy’s spectrum and fit an early-type galaxy template spectrum from the stellar-population synthesis models of Bruzual & Charlot (2003). The template spectrum is a combination of a 0.3 Gyr, solar metallicity, young stellar population and a 7 Gyr, solar metallicity, old stellar population, based on Yan et al. (2006).

For each galaxy spectrum, we subtract off the continuum and then calculate the flux of the  $\text{H}\beta$  and [O III]  $\lambda 5007$  emission lines by summing the one-dimensional spectrum over a  $30 \text{ \AA}$  window ( $\sim 18 \text{ \AA}$  in the rest frame) around each peak. We note that our continuum subtraction accounts for any  $\text{H}\beta$  absorption, enabling an accurate measurement of the  $\text{H}\beta$  emission-line flux. We compute rest-frame  $U - B$  colors and  $M_B$  absolute magnitudes using a K-correction code developed for DEEP2 galaxies (Willmer et al. 2006).

We make a series of cuts to the full set of DEEP2 galaxies to identify those hosting AGNs. First, DEEP2 spectra typically cover the range 6500 – 9500 Å, so our sample size is limited by the requirement that both  $\text{H}\beta$  and [O III] lines are within that window. This restricts

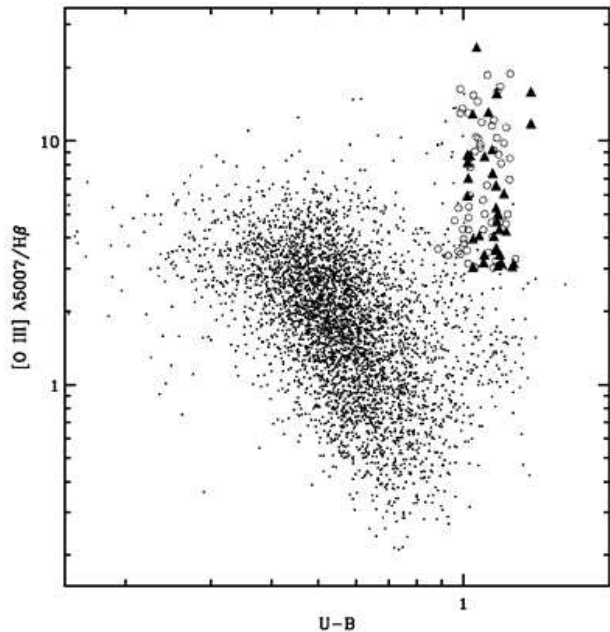


FIG. 1.— [O III]  $\lambda 5007/H\beta$  line flux ratios and rest-frame  $U-B$  colors for our sample of DEEP2 galaxies. Points show the galaxies with accurate redshift measurements (quality  $Q = 3$  or 4; see Davis et al. 2007) and measurable [O III]  $\lambda 5007/H\beta$  ratios; open circles show the red galaxies hosting AGNs, selected by [O III]  $\lambda 5007/H\beta > 3$  and  $U-B > -0.032(M_B - 5 \log h + 21.62) + 1.285 - 0.25$  (note that because of the dependence on absolute magnitude  $M_B$ , this does not correspond to a simple cut in this figure); and filled triangles show the 32 offset and dual AGNs, which are the red galaxies that host AGNs with  $> 3\sigma$  velocity offsets relative to the host galaxy stars.

us to a redshift range  $0.34 < z < 0.82$ , which is outside of the bulk of the DEEP2 sample. Second, to ensure that line emission is the result of AGN activity and not star formation, we require that our sample has rest-frame  $U-B$  colors  $U-B > -0.032(M_B - 5 \log h + 21.62) + 1.285 - 0.25$ , consistent with a red-sequence galaxy spectrum (Willmer et al. 2006). These first two cuts yield a parent sample of 1881 red galaxies with an absolute magnitude range of  $-22.7 < M_B - 5 \log h < -16.8$ .

Next we identify which of these red galaxies host AGNs. First, we require that [O III]  $\lambda 5007$  line emission be detected with at least  $3\sigma$  significance, providing an indication of possible AGN activity. Second, to ensure that we can robustly measure the [O III]  $\lambda 5007$  emission line redshift, we require [O III]  $\lambda 5007$  equivalent width  $> 2 \text{ \AA}$ . Finally, we require that candidates have line flux ratios [O III]  $\lambda 5007/H\beta > 3$  to distinguish Seyferts from other line-emitting galaxies (Baldwin et al. 1981; Kauffmann et al. 2003; Yan et al. 2006). Of the parent sample of 1881 red galaxies, 91 of them host AGNs as determined by these criteria. We do not limit our sample by Seyfert type.

Figure 1 illustrates the differences between the population of red galaxies hosting AGNs and the general population of galaxies. Galaxies populate this diagram of [O III]  $\lambda 5007/H\beta$  versus  $U-B$  similar to the way they populate the traditional BPT diagram of

[N II]  $\lambda 6583/H\alpha$  versus [O III]  $\lambda 5007/H\beta$ , disassociating into a star-forming sequence and an AGN plume. The separation between these populations is less distinct here than in the BPT diagram, but the figure illustrates that we have selected a well-defined sample of galaxies that are well separated from the main star-forming sequence.

## 2.2. Measurement of AGN Velocity Offsets

The line width of AGN [O III] emission usually correlates with the velocity dispersion of the stellar bulge of the host galaxy, implying that the [O III] emission component is generally at rest with respect to the stellar bulge and, by extension, the central SMBH (Greene & Ho 2005). In that case, the [O III] emission lines should be at the same redshift as the stellar component of the host galaxy. If two galaxies with central SMBHs have recently undergone a merger, however, the merger remnant should host two SMBHs moving relative to one another. If one or both of the SMBHs are active, we expect the AGN [O III] emission lines to be at a different redshift than the remnant’s stars, whose mean velocity will be in the rest frame of the remnant.

To identify such cases, we first measure the galaxy redshift based on the wavelengths of the diversity of absorption features in the stellar spectrum. We accomplish this by fitting template spectra to the observed spectra, as described in Section 2.1. We then determine the redshift that yields minimum  $\chi^2$  for the fit of the galaxy template spectrum to the actual spectrum. In performing this fit, we include the variance in the one-dimensional spectrum at each wavelength position. We compute the variance by propagating errors from the Poisson uncertainty in photon counts on each pixel of the detector, including the effects of night-sky background and cosmic rays. Our sky subtraction does not introduce significant systematic errors beyond this simple Poisson noise (Faber et al., in preparation). We determine the uncertainty in the absorption redshift as the width of the  $\chi^2$  minimum at which  $\Delta\chi^2 = 1$ .

Then, we measure the emission redshift using a robust two-step centroiding algorithm. First, we take a  $30 \text{ \AA}$  window ( $\sim 18 \text{ \AA}$  in the rest frame) around each galaxy’s [O III]  $\lambda 5007$  emission line and fit a Gaussian to the line. We use the width of this Gaussian to define a narrow window centered on the peak of the emission line, within which we compute the line centroid. This procedure gives a centroid measurement whose value is robust to noise in the outer wings of the line. Using Monte Carlo realizations drawn from the variance in the spectra, we find that our centroid values are accurate to better than  $0.1 \text{ \AA}$  for typical signal-to-noise ratios.

We then verify each galaxy’s absorption and emission-line redshift by eye, and in the process reject the 5% of objects in which the fit appears to be dominated by noise and the signal-to-noise ratio is too low to accurately determine an absorption redshift.

A discrepancy between absorption and emission redshifts could indicate that the [O III] emission component (the AGN) is moving with respect to the absorption component (the host galaxy’s stars). We convert the redshift difference to a radial velocity separation in the host’s rest frame, and we derive the error on this velocity separation from the errors on the two redshifts. With these velocity separations, we identify offset and dual AGNs.

TABLE 1  
HOST GALAXY PROPERTIES OF THE 32 OFFSET AND DUAL AGNS

ID	$U-B$	$M_B$ $-5 \log h$	[O III] $\lambda 5007/$ $H\beta$	$z_{abs}$	$z_{em}$	$v_{em} - v_{abs}$ ( $\text{km s}^{-1}$ )
EGSD2 J141515.6+520354	1.04	-20.9	12.9	0.69304	0.69355	$89.9 \pm 14.6$
EGSD2 J141417.6+520351	1.10	-20.5	3.18	0.77447	0.77404	$-72.9 \pm 17.7$
EGSD2 J141523.5+520532	1.20	-20.3	3.16	0.48214	0.48265	$103.9 \pm 16.9$
EGSD2 J141550.8+520929	1.17	-20.6	4.69	0.61987	0.61935	$-97.0 \pm 19.8$
			3.58		0.62171	$339.5 \pm 19.8$
EGSD2 J141547.7+520843	1.08	-20.9	4.09	0.61916	0.61806	$-203.0 \pm 20.6$
EGSD2 J141458.0+520915	1.18	-19.3	3.08	0.48358	0.48396	$76.1 \pm 19.6$
EGSD2 J141433.1+520834	1.17	-20.9	5.34	0.77156	0.77261	$178.7 \pm 22.6$
EGSD2 J141643.2+521721	1.26	-20.4	3.06	0.45095	0.45133	$77.0 \pm 11.5$
EGSD2 J141732.6+523817	1.19	-22.0	3.43	0.71671	0.71792	$211.5 \pm 12.1$
EGSD2 J141711.0+523729	1.18	-21.1	4.36	0.64395	0.64344	$-92.1 \pm 20.3$
EGSD2 J141839.2+525140	1.17	-20.3	3.65	0.34514	0.34546	$71.4 \pm 18.4$
EGSD2 J142017.9+525538	1.02	-18.7	5.98	0.63750	0.63843	$169.9 \pm 30.0$
EGSD2 J142043.0+525716	1.18	-19.7	5.06	0.74898	0.74831	$-115.0 \pm 24.9$
EGSD2 J142033.6+525917	1.38	-20.2	11.8	0.70882	0.70701	$-318.3 \pm 34.1$
			15.9		0.71060	$311.0 \pm 34.1$
EGSD2 J141939.0+530223	1.05	-20.2	3.04	0.76309	0.76243	$-111.4 \pm 30.4$
EGSD2 J141929.7+530104	1.10	-21.7	3.42	0.67789	0.67727	$-110.9 \pm 13.2$
EGSD2 J142010.1+530738	1.15	-20.4	4.07	0.57380	0.57468	$167.6 \pm 32.7$
EGSD2 J142153.6+531352	1.02	-20.7	8.20	0.67257	0.67205	$-93.9 \pm 18.3$
EGSD2 J142057.2+531104	1.21	-20.0	6.09	0.71417	0.71372	$-78.8 \pm 17.3$
EGSD2 J142143.0+531820	1.17	-20.8	6.58	0.76479	0.76501	$37.1 \pm 12.3$
DEEP2 J164714.9+350405	1.22	-20.3	4.28	0.76186	0.76147	$-65.7 \pm 14.7$
DEEP2 J164646.6+350648	1.02	-20.8	8.82	0.74588	0.74629	$69.2 \pm 13.5$
DEEP2 J165128.8+344841	1.03	-20.8	8.75	0.70433	0.70381	$-90.7 \pm 16.5$
DEEP2 J232717.4+000803	1.15	-20.4	$>9.24^a$	0.74173	0.74142	$-54.3 \pm 16.9$
DEEP2 J232907.8+001742	1.06	-21.4	24.3	0.79166	0.79137	$-47.8 \pm 6.3$
DEEP2 J233030.0+002418	1.02	-21.0	7.05	0.77831	0.77922	$153.7 \pm 15.6$
DEEP2 J233250.1+001929	1.11	-20.2	8.65	0.70228	0.70291	$110.1 \pm 22.4$
DEEP2 J022735.0+003816	1.13	-20.5	13.1	0.67491	0.67449	$-75.7 \pm 16.2$
DEEP2 J023050.3+002408	1.15	-20.6	7.39	0.62009	0.62063	$100.4 \pm 16.5$
DEEP2 J023059.6+004418	1.05	-20.1	3.97	0.77672	0.77618	$-90.4 \pm 20.6$
DEEP2 J022907.1+004353	1.17	-21.3	15.7	0.65378	0.65299	$-143.0 \pm 16.0$
DEEP2 J023121.3+005110	1.27	-22.7	3.15	0.77503	0.77665	$273.9 \pm 8.5$

<sup>a</sup> For this object, the measurement of  $H\beta$  flux is consistent with zero, so we use the  $2\sigma$  upper limit on  $H\beta$  to derive a lower limit for [O III]  $\lambda 5007/H\beta$ .

### 2.3. 32 Offset and Dual AGNs

To avoid contamination from objects with nonzero velocity differences due to measurement errors, we restrict our offset AGN sample to only those with velocities different from zero by more than  $3\sigma$ , which excludes all cases with differences  $\lesssim 50 \text{ km s}^{-1}$ . We are sensitive to relatively small velocity differences due to the high spectral resolution ( $R \sim 5000$ ) and excellent sky subtraction of DEEP2 data. Absorption-line redshift uncertainties estimated from the width of the  $\chi^2$  minimum (described in Section 2.2) are small:  $6 - 34 \text{ km s}^{-1}$  for our sample, with a median of  $17 \text{ km s}^{-1}$ . Uncertainties in the [O III] emission-line redshifts (described in Section 2.2) are even smaller,  $\lesssim 1 \text{ km s}^{-1}$ . These errors are statistical only; they do not include systematic errors that arise from, for example, a galaxy not being perfectly centered in its slit. However, to first order position errors will have an identical effect on the observed velocity of a galaxy and any AGN it harbors.

As a check on our error estimates, we have compared the differences between the AGN emission redshift and the host galaxy absorption redshift for the three AGN host galaxies observed twice by DEEP2; the different observations yield velocity offsets differing by  $4.2 \text{ km s}^{-1}$ ,  $9.4 \text{ km s}^{-1}$ , and  $15.2 \text{ km s}^{-1}$ . Hence, we can find no evidence that our redshift uncertainties have been significantly underestimated.

After we reject the 59 galaxies with measured velocity differences below  $3\sigma$  significance, the final sample consists of 30 offset AGNs and two dual AGNs, for a total of 32 objects. This number is a lower bound on the true number of offset and dual AGNs in the sample, because we exclude low-significance velocity offsets and are also not sensitive to velocity components perpendicular to the line of sight. We do not select by Seyfert type, but all 32 offset and dual AGNs are in Seyfert 2 galaxies.

Figure 1 shows that the offset and dual AGNs do not have systematically different [O III]  $\lambda 5007/H\beta$  ratios or colors from the general population of AGNs, but rather are uniformly distributed. Apart from their velocity offsets, the offset and dual AGNs appear to be typical Seyferts. Table 1 gives the rest-frame  $U-B$  colors, absolute magnitudes, [O III]  $\lambda 5007/H\beta$  ratios, absorption and emission redshifts, and velocity offsets for each of the 32 offset and dual AGNs.

Figure 2 shows a histogram of the difference between the velocity of the emission component (the AGN) and the absorption component (the host galaxy's stars) for the 32 offset and dual AGNs. Because the histogram is symmetric about zero velocity difference, we see no evidence for bias in the radial direction of the velocity of the emission-line region. The dotted histogram shows the 59 AGNs that exhibit less than  $3\sigma$  velocity differences, preventing their classification as offset AGNs.

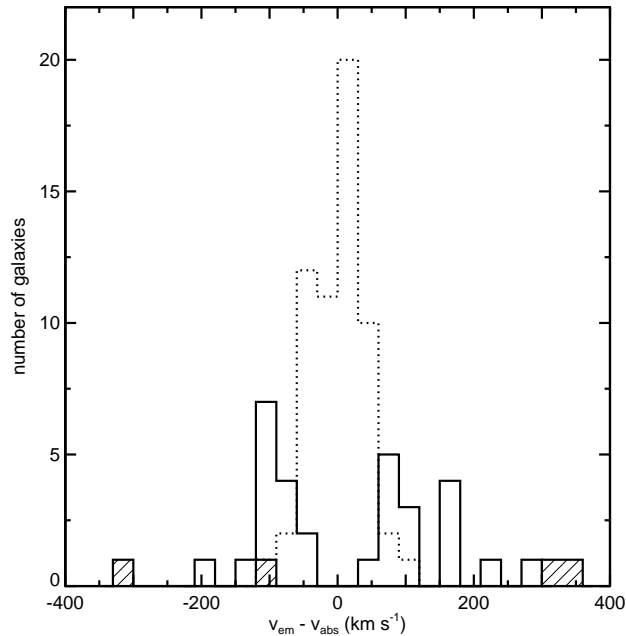


FIG. 2.— Differences between the velocity of AGN emission lines ( $v_{em}$ ) and the velocity of the host galaxy’s stars ( $v_{abs}$ ) for the full sample of 91 AGNs. The open histogram depicts the velocity differences of the 30 offset AGNs, the hatched histogram depicts the velocity differences for each component of the two dual AGNs, and the dotted histogram depicts the 59 objects with less than  $3\sigma$  velocity difference that were removed from our sample to eliminate contamination due to measurement errors from objects with no statistically significant velocity difference. The velocity-difference distribution of the remaining AGNs is symmetric, indicating that an offset AGN emission line is equally likely to be redshifted or blueshifted relative to the rest frame of the stellar continuum.

Figure 3 depicts example offset and dual AGNs plotted in the rest frame of the stellar continuum, where the dashed lines show the expected locations of the [O III]  $\lambda\lambda$  4959, 5007 emission lines in that rest frame. The bottom six spectra (shown in red) are example spectra for six offset AGNs, where for clarity we set off each spectrum vertically from the others. The plot shows AGNs that are both blueshifted and redshifted with respect to their host galaxies, ranging from a blueshift of  $-143 \text{ km s}^{-1}$  to a redshift of  $170 \text{ km s}^{-1}$ .

The top two spectra (shown in black) in Figure 3 depict the two dual AGNs in our sample. The multislit spectroscopy used in the DEEP2 survey also enables us to make two-dimensional spectra of spatial position and wavelength for each galaxy. The slits are  $1''$  wide and vary in length from typically  $\sim 5''$  to  $\sim 10''$ . Figure 4 shows the two-dimensional DEEP2 spectrum centered around each object’s [O III]  $\lambda 5007$  emission. Each dual AGN has double-peaked emission at [O III]  $\lambda 5007$ , and we determine the spatial centroid of each emission component by applying the technique described in Section 2.2 for measuring the emission redshift, only we apply this technique along the spatial direction of the two-dimensional spectrum rather than the wavelength direction.

The dual AGN EGSD2 J142033.6+525917 at redshift  $z = 0.71$  is shown at the top of Figure 4. Its spectrum

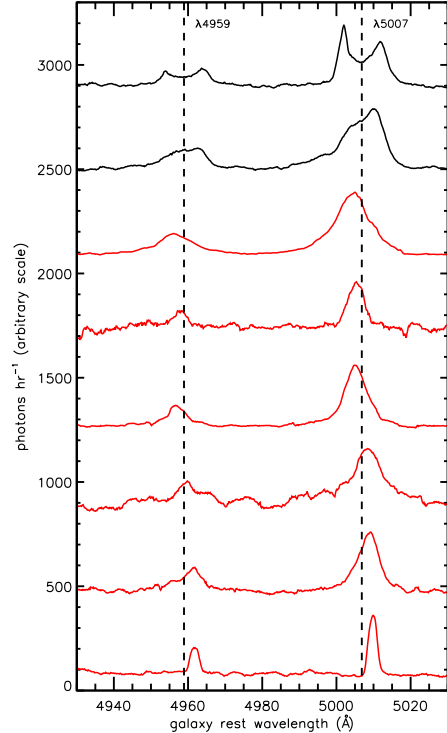


FIG. 3.— Segments of the one-dimensional DEIMOS spectra of the host galaxies of the two dual AGNs (shown as the top two, in black) and six typical offset AGNs (shown as the bottom six, in red). For clarity, the spectra are offset from one another vertically and normalized to span 300 counts  $\text{hr}^{-1}$ . Each spectrum is shifted to the rest frame of the host galaxy’s stars, weighted by its inverse variance, and smoothed by a smoothing length of  $1.5 \text{ \AA}$ . The dashed lines show the expected wavelengths of [O III] at 4959  $\text{\AA}$  and 5007  $\text{\AA}$ . From top to bottom, the spectra shown are of EGSD2 J142033.6+525917, EGSD2 J141550.8+520929, DEEP2 J022907.1+004353, EGSD2 J142043.0+525716, EGSD2 J142153.6+531352, EGSD2 J141515.6+520354, DEEP2 J233250.1+001929, and EGSD2 J142017.9+525538. From top to bottom, the velocity separations between the two [O III] emission line peaks in the dual AGNs are  $630 \text{ km s}^{-1}$  and  $440 \text{ km s}^{-1}$ , while the velocity offsets for the [O III] emission lines in the offset AGNs are  $-140 \text{ km s}^{-1}$ ,  $-120 \text{ km s}^{-1}$ ,  $-94 \text{ km s}^{-1}$ ,  $90 \text{ km s}^{-1}$ ,  $110 \text{ km s}^{-1}$ , and  $170 \text{ km s}^{-1}$ .

features double-peaked [O III] emission lines separated by  $630 \text{ km s}^{-1}$  in the host rest frame (Gerke et al. 2007). From the two-dimensional DEIMOS spectrum of the object, the projected physical separation between the pair of emission peaks is 1.5 DEIMOS pixels, or  $0''.17$ , which corresponds to a projected physical separation of  $0.84 h^{-1} \text{ kpc}$ .

The dual AGN EGSD2 J141550.8+520929 at  $z = 0.62$  is shown at the bottom of Figure 4. Its two-dimensional DEEP2 spectrum shows two overlapping [O III] emission lines. The velocity separation between the two emission components is  $440 \text{ km s}^{-1}$  and the spatial offset of their centroids is 3.1 DEIMOS pixels, or  $0''.34$ , which corresponds to a projected physical separation of  $1.6 h^{-1} \text{ kpc}$ .

#### 2.4. Extrapolated Number of Low-Velocity-Offset AGNs

By excluding objects with less than  $3\sigma$  significance, we will discard many AGNs with small, but real, velocity offsets. We can measure only the radial component of a velocity, which is a factor of  $\sin i$  less than the to-

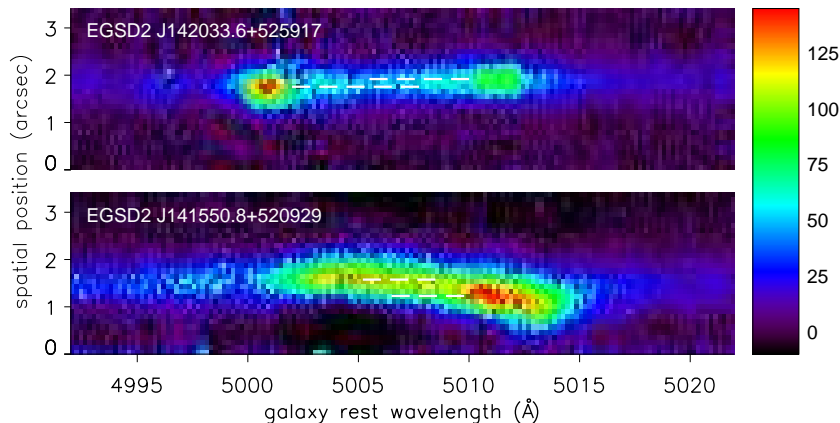


FIG. 4.— [O III]  $\lambda 5007$  emission in the two-dimensional DEIMOS spectra of the two dual AGNs, with night-sky emission features subtracted. The top panel depicts EGS2 J142033.6+525917 at  $z = 0.71$ , and the bottom panel depicts EGS2 J141550.8+520929 at  $z = 0.62$ . In both panels, the vertical axis spans 32 DEIMOS pixels ( $3''.5$ ) in spatial position along the slit and the horizontal axis spans 30  $\text{\AA}$  in rest-frame wavelength centered on [O III]  $\lambda 5007$ . The horizontal, white dashed lines show the spatial centroids of each emission-line component. The two emission-line components in the top panel are separated by 1.5 DEIMOS pixels, which is equivalent to  $0''.17$  or  $0.84 h^{-1} \text{ kpc}$ , and the two emission-line components in the bottom panel are separated by 3.1 DEIMOS pixels, which is equivalent to  $0''.34$  or  $1.6 h^{-1} \text{ kpc}$ . The slanted, nearly-vertical features are imperfectly subtracted night-sky lines, and the color bar provides a scale for flux in counts/hour/pixel.

tal velocity at an angle of inclination  $i$  relative to the perpendicular to the line of sight. Because of these projection effects, we expect an even greater abundance of small measured velocity offsets than large measured offsets. If we fit a Gaussian centered at zero to the offset AGN velocity distribution shown in Figure 2, we find that 23 objects with absolute velocity offsets  $< 50 \text{ km s}^{-1}$  should be added to the sample to create a Gaussian distribution of velocity offsets.

More conservatively, we can assume that the velocity-offset distribution is flat in the central region around zero. If we assume the number of offset AGNs with absolute velocity offsets  $< 50 \text{ km s}^{-1}$  is determined by the mean number of offset AGNs with absolute offsets ranging from  $50 - 75 \text{ km s}^{-1}$ , this would instead increase the sample size by eight objects with  $< 50 \text{ km s}^{-1}$  absolute velocity offsets.

We add 23, or more conservatively eight, low-velocity-offset AGNs to the 32 definitively detected offset and dual AGNs. As a result, we expect 40 – 55 offset and dual AGNs in our full sample of 91 AGNs.

### 3. INTERPRETATION OF OFFSETS

We have measured statistically significant velocity offsets of [O III] emission lines in 32 offset and dual AGNs in DEEP2 red galaxies. Here, we explore the physical mechanisms that could cause the [O III] velocity offsets we observe: small-scale gas kinematics, AGN outflows and jets, recoiling SMBHs due to gravitational radiation emission after SMBH coalescence, and inspiralling SMBHs in a galaxy merger. We find that the most plausible explanation for our offset and dual AGNs is inspiralling SMBHs in a galaxy merger remnant.

#### 3.1. Small-scale Gas Kinematics

Gas rotation and bulk flows on small scales can produce velocity shifts in [O III] emission lines. Here we review observations of [O III] velocity shifts that can

be explained by small-scale gas kinematics and examine whether such effects could explain the velocity offsets in our sample.

In an analysis of 13 Seyfert galaxies and quasi-stellar objects (QSOs) at  $0.003 < z < 0.04$ , Vrtilik & Carleton (1985) measured [O III] emission-line velocity offsets ranging from  $0 - 180 \text{ km s}^{-1}$ . Five of the 13 galaxies have [O III] velocity offsets greater than  $3\sigma$  in significance, which is our definition of an offset AGN (Section 2.3). Of the five Seyferts with statistically significant [O III] velocity offsets, three exhibit redshifted [O III] and two exhibit blueshifted [O III]. These observations were taken with an echelle spectrograph. If the slits were slightly miscentered on the galaxy centers, then rotation of gas in disks of order 100 pc in size or small-scale bulk flows of gas near the galaxy centers could produce the [O III] velocity offsets measured by Vrtilik & Carleton (1985).

In addition, observations of 54 Seyferts at  $0.002 < z < 0.04$  revealed [O III] emission-line velocity offsets of  $1 - 230 \text{ km s}^{-1}$  (Nelson & Whittle 1995). 25/54 of the velocity offsets have greater than  $3\sigma$  significance, and of these six exhibit redshifted [O III] and 19 exhibit blueshifted [O III]. These velocity offsets could be explained by slit miscentering and small-scale gas kinematics, as described above. However, because there are a factor of 3 more blueshifts than redshifts, AGN outflows may be the likelier explanation (Section 3.2).

For completeness, we also note that although some analyses of double-peaked broad lines in quasar spectra conclude they are caused by binary black holes (e.g., Gaskell 1984, 1988, 1996), most such lines are now understood to be caused by accretion discs (e.g., Eracleous et al. 1997; Eracleous & Halpern 2003). However, these are a very different class of objects than our sample of double-peaked AGNs. The quasar sample exhibits emission from the BLR on  $\sim 1 \text{ pc}$  scales that produces double-peaked broad lines with line widths com-

parable to their velocity separations, whereas our dual AGNs exhibit emission from the NLR on  $\sim 100$  pc scales that produce double-peaked narrow lines with line widths smaller than their velocity separations. Because we probe different sets of lines that arise from much larger scales, the interpretations of the double-peaked broad lines do not necessarily transfer to our sample of dual AGNs.

Though they are a possible explanation for the Vrtilek & Carleton (1985) and Nelson & Whittle (1995) velocity offsets and the double-peaked broad line quasar spectra, small-scale gas rotation or small-scale bulk flows of gas alone cannot explain our observations of [O III] velocity offsets. Our observations are at the much higher redshift range  $0.34 < z < 0.82$ , where our  $1''$  slit width subtends several kpc across each galaxy. As a result, our observations are based on a full spatial average of the NLR kinematics, which means that small-scale gas kinematics alone cannot cause the [O III] velocity offsets we measure.

If the small-scale gas kinematics were accompanied by local dust, one can imagine scenarios where only the blueshifted (redshifted) gas is obscured, leaving the redshifted (blueshifted) gas to manifest as velocity-offset emission lines. However, for this scenario to occur the local dust would need to be pathologically patchy rather than in the usual form of a ring or torus. Dust on larger scales, such as in a disk or lane on kpc or 10 kpc scales, would blot out the entire central region and result in no velocity-offset detection.

While small-scale gas kinematics can lead to observations of [O III] velocity offsets at low redshifts, they cannot alone produce the velocity offsets we measure at higher redshifts. A combination of small-scale gas kinematics and patchy dust could explain our velocity offsets, though the dust must be in an unusual configuration.

### 3.2. AGN Outflows and Jets

Velocity shifts of [O III] emission lines can also be explained by a strong, decelerating wind in the inner NLR of the AGN (Komossa et al. 2008a). For a galactic wind, unlike a stellar wind, the mass enclosed increases as the galactic wind flows outward, and causes the galactic wind to decelerate with distance from the galactic center. Studies of outflows suggest that the NLR around the AGN is stratified such that high-ionization lines, such as [O III], are preferentially generated near the AGN and low-ionization lines, such as  $H\beta$  and [O II], are preferentially generated further from the AGN (e.g., Zamanov et al. 2002; Komossa et al. 2008a). These outflow studies find that a centrally driven outflow that decelerates with distance from the AGN would impart the highest velocities to the nearby high-ionization lines, and low-ionization lines further from the AGN would exhibit lower velocity offsets or remain stationary with respect to the galaxy's stellar component.

If the AGN has a bulk motion within the host galaxy, however, then all AGN emission lines, regardless of ionization potential, would exhibit the same velocity shifts relative to the host galaxy's stars. While only nine galaxies in our sample have [O II] lines within our wavelength window of observation and 31 have sufficiently high  $H\beta$  signal-to-noise ratios to accurately determine a redshift, in galaxies where the measurements are possible we find

that [O II],  $H\beta$ , and [O III] lines have consistent velocity offsets to within  $1\sigma$ . These AGNs all exhibit bulk motions not consistent with the stratified velocity structure of outflows.

We also compare to other samples of AGNs exhibiting velocity offsets due to outflows to understand the physical mechanism behind our offsets. For a sample of  $\sim 200$  quasars at  $z < 0.8$ , Zamanov et al. (2002) measured the [O III]  $\lambda 5007$  redshift relative to the  $H\beta$  redshift, taken to be the systemic redshift of the galaxy. In such luminous objects, stellar absorption features are overwhelmed by light from the quasar. As a result, the host galaxy redshift cannot be derived from the stellar absorption lines as we do with the DEEP2 sample. Of the objects with inconsistent [O III]  $\lambda 5007$  and  $H\beta$  redshifts, more had blueshifted [O III]  $\lambda 5007$  than redshifted [O III]  $\lambda 5007$ , relative to  $H\beta$ . This includes a factor of 3 more blueshifts of radial velocity  $v_r$  in the range  $-200 \text{ km s}^{-1} \lesssim \Delta v_r \lesssim -100 \text{ km s}^{-1}$  than redshifts of  $100 \text{ km s}^{-1} \lesssim \Delta v_r \lesssim 200 \text{ km s}^{-1}$ . AGN outflows are expected to exhibit blueshifts, as material traveling away from the observer will be on the far side of the AGN and obscured by its dust torus. The outliers with blueshifted [O III]  $\lambda 5007$  also extended out to  $\Delta v_r \approx -1000 \text{ km s}^{-1}$ , while no redshifted [O III]  $\lambda 5007$  was observed beyond  $\Delta v_r \approx 280 \text{ km s}^{-1}$ . Because the distribution of velocity offsets is skewed toward the blue, Zamanov et al. (2002) concluded that outflows in the inner NLR of the AGN influence the peak velocity of the [O III]  $\lambda 5007$  line. The Nelson & Whittle (1995) sample also has a velocity distribution skewed toward the blue, suggesting that outflows may be the root of those velocity offsets.

In our sample, however, there are equal numbers of blueshifted and redshifted outliers (15 of each) and both blueshifted and redshifted outlier distributions extend to similar velocity offsets ( $\Delta v_r = -203 \text{ km s}^{-1}$  and  $\Delta v_r = 274 \text{ km s}^{-1}$ , respectively). Because the distribution of [O III]  $\lambda 5007$  velocity offsets in our sample is quite different from that of Zamanov et al. (2002), the physical explanations for the offsets in the two samples are likely different.

Furthermore, outflows are generally found to cause a strong correlation of increasing [O III] line width with [O III] blueshift (e.g., Komossa et al. 2008a). By contrast, our sample has a correlation coefficient of 0.009, indicating a very weak correlation between [O III] line width and [O III] velocity shift.

To explore how small-scale outflows would affect observations of our high-redshift Seyfert galaxies, we examine nearby Seyfert galaxies with outflows on scales of 100 pc. Using the *Hubble Space Telescope* Imaging Spectrograph (STIS), Das et al. (2006) obtained spatially resolved spectroscopy of outflowing gas in the NLR of the Seyfert 2 galaxy NGC 1068. The outflowing clouds produce a complicated velocity structure in the [O III] emission lines, with multiple emission components having velocity offsets (both blueshifts and redshifts) up to several hundred  $\text{km s}^{-1}$ . This velocity structure is confined to the inner  $\sim 100$  pc of the emitting region; outside of this, the outflow velocity drops and reaches zero at  $\sim 300$  pc. (Similar kinematics and spatial structure are seen in the Seyfert 1 galaxy NGC 4151; Das et al. 2005.) By comparison, a DEEP2 slit of  $1''$  width subtends approximately 7 kpc at  $z \sim 0.7$  (where most of our sample

lies) and a DEIMOS pixel subtends approximately 1 kpc, so similar kinematics on subkiloparsec scales would not be resolved in our observations. To get a rough approximation of what the spectrum of a system like NGC 1068 would look like in DEEP2, we can coadd the neighboring STIS spectra of NGC 1068 from Das et al. (2006); this yields a broadened [O III] emission line with a blue wing but no large overall offset in the velocity of its peak.

Another example of small-scale outflows is the Ruiz et al. (2005) sample, which consists of STIS observations of 10 Seyfert galaxies at  $0.003 < z < 0.03$ . Six of the 10 objects have observable [O III] velocity offsets, ranging from 70 – 200 km s<sup>-1</sup>. The disturbed kinematics of these galaxies result in [O III] FWHMs that are generally larger than the [O III] velocity offsets, and such increases in [O III] FWHM may also be the result of radio jets driving the outflows (Nelson & Whittle 1996).

Our sample of offset and dual AGNs does not exhibit this trend of larger [O III] FWHMs than velocity offsets, and our approximation of NGC 1068 at a higher redshift suggests that we would not detect a velocity offset in such an object. As a result, the nearby systems we examine show no evidence that typical small-scale Seyfert outflows would lead to the kind of emission-line offsets we observe in our sample.

To understand the effect of large-scale outflows on observations of our sample of Seyferts, we consider nearby Seyfert galaxies with outflows on scales of 10 kpc. These systems exhibit disturbed kinematics, with [O III] velocity dispersions that are larger than the [O III] velocity offsets (e.g., Veilleux et al. 2001; Geressen et al. 2009), but this effect is not seen in our offset and dual AGNs. Also, in the local systems the outflowing regions tend to be much fainter than the stationary central NLR. In a composite spectrum of such an object at the redshift of our sample, the [O III] flux would be dominated by the brighter, stationary central component and we might not detect a velocity offset.

Another scenario is that dust in the galaxy, in concert with an outflow, could result in a detection of an [O III] velocity offset. As described above, a local dust torus would result in an excess of [O III] blueshifts rather than our sample’s symmetric distribution of [O III] redshifts and blueshifts. Dust on larger scales that obscures only a portion of the outflow could result in the observation of an [O III] velocity offset, but such configurations of dust have not been seen locally. Further, our sample consists of red galaxies that should not have much dust, and AGNs that are luminous enough to drive large-scale outflows would also likely expel dust. Even if a conspiracy between dust and large-scale outflows led to observations of [O III] velocity offsets, the [O III] velocity dispersions would still be larger than the velocity offsets, which is not the case in our sample.

Our above comparisons to local galaxies with small-scale or large-scale outflows suggest that the [O III] velocity offsets in our sample are not consistent with the outflow explanation. However, a combination of partial dust obscuration and outflow activity, however unlikely, could explain the velocity offsets we observe.

### 3.3. Recoiling SMBHs

Another possible interpretation of our offset AGNs is that some may be recoiling SMBHs. After a galaxy

merger two SMBHs can coalesce due to gravitational wave emission, which can carry away linear momentum and impart a velocity kick of typically tens to hundreds of km s<sup>-1</sup> to the resultant merged SMBH (Peres 1962; Bekenstein 1973). The BLR could remain bound to the recoiling SMBH, but the NLR would remain with the host galaxy (Merritt et al. 2006; Bonning et al. 2007). A recoiling SMBH could carry with it an accretion disk of nuclear stars and gas from the BLR, which could power AGN activity for  $\sim 100$  Myr (e.g., Merritt et al. 2004; Loeb 2007; Bonning et al. 2007). As a result, recoiling SMBHs could be visible as AGNs with BLR velocity offsets relative to the NLR and the host galaxy. A search of the Sloan Digital Sky Survey for QSOs with such offsets found no convincing candidates (Bonning et al. 2007), and the subsequent discovery of a Sloan QSO with a 2650 km s<sup>-1</sup> offset (Komossa et al. 2008b) may in fact be a SMBH binary (Bogdanović et al. 2009; Dotti et al. 2008) or a superposition of two AGNs (Shields et al. 2009) rather than a recoiling SMBH. Our offset AGNs are Seyfert 2 galaxies with velocity offsets of the NLR emission lines, which does not fit the recoiling SMBH paradigm of a shifted BLR and stationary NLR.

### 3.4. Offset and Dual AGNs Are Most Likely the Result of Galaxy Mergers

We find no significant evidence that the velocity offsets in our sample are the result of small-scale gas kinematics, AGN outflows or jets, or recoiling SMBHs, but a combination of gas kinematics or outflows with an unexpected distribution of dust could produce the [O III] velocity offsets we measure. Although some fraction of the [O III] velocity offsets in our sample might be caused by gas kinematics or outflows, these effects are unlikely to explain all of our objects unless the population of AGNs at  $z \sim 0.7$  is qualitatively different from the well-studied local population.

Rather, the most plausible explanation for our observations of offset [O III] lines is an AGN moving with respect to the host galaxy as the result of a merger. Inspiralling SMBHs are expected to exist as a consequence of the well-established evidence for galaxy mergers and galaxies hosting central SMBHs. NGC 3341, a disturbed disk galaxy at  $z = 0.0271$  with a Seyfert 2 nucleus at a spatial offset of 5.1 kpc and a blueshifted velocity of 190 km s<sup>-1</sup> relative to the primary galaxy (Barth et al. 2008), is a local example of a galaxy merger hosting inspiralling SMBHs. Whereas none of the local observations of velocity offsets we explored in Sections 3.1 and 3.2 would translate into observable velocity offsets at our redshift range, the Barth et al. (2008) object would. Because inspiralling SMBHs are an expected consequence of galaxy mergers and because our offset and dual AGNs are consistent with the observational signatures expected of inspiralling SMBHs, we conclude that our observed [O III] velocity offsets are most likely the result of inspiralling SMBHs in galaxy mergers.

## 4. RESULTS AND DISCUSSION

Based on our interpretation that the observed offset and dual AGNs are the result of mergers, we now use our sample to estimate the fraction of AGNs hosted by red galaxy mergers and the red galaxy merger rate.



#### 4.1. Evidence for a Link between AGN Activity and Galaxy Mergers

Combining the extrapolated number of small-velocity-offset AGNs (as detailed in Section 2.4) with our 32 definitively detected offset and dual AGNs, we expect a total of 40 – 55 offset and dual AGNs in our data. Our interpretation of these objects as merger remnants, therefore, implies that of the 91 red galaxies harboring AGNs in DEEP2 at  $0.34 < z < 0.82$ , roughly half of the AGNs are moving relative to their host galaxies due to a recent merger. This striking result, that approximately half of the red galaxies hosting AGNs are also merger remnants, suggests a strong link between AGN activity and red galaxy mergers.

A number of mechanisms could explain this. During a galaxy merger the hot gas of the intergalactic medium is shock heated and cools by radiation, forming cooling flows that can fuel an AGN. Numerical simulations show that mergers between gas-rich, late-type galaxies can trigger nuclear gas flows that power two separated AGNs that then merge to form a single central AGN (Springel et al. 2005a), and gas-poor, red galaxy mergers might have enough gas to fuel AGNs in the same way. Galaxy mergers can also trigger starbursts, and after tens of Myr some stars evolve into asymptotic giant branch stars, whose winds might be accreted efficiently onto SMBHs to fuel AGNs (Davies et al. 2007).

Morphologies based on the imaging of quasar host galaxies also suggest that  $\sim 30\%$  of quasars reside in host galaxies that show evidence of interactions and mergers (Marble et al. 2003; Guyon et al. 2006). More recently, Urrutia et al. (2008) found that 85% of dust-reddened quasars show evidence of merging in images of their host galaxies. Our results are roughly consistent with this finding, though the two samples are very different. Our Seyfert 2 AGNs are relatively low luminosity in comparison to quasars, and the dynamical state of the SMBHs in the quasar host galaxies is unknown. We find that AGN activity can be triggered in merging SMBHs even before coalescence.

#### 4.2. Galaxy Merger Rates

Assuming that all of our offset and dual AGNs are merger remnants, and making no other assumptions, we set a hard lower limit that at least 2% of DEEP2 red galaxies at  $0.34 < z < 0.82$  have undergone a merger in the previous  $\sim 100$  Myr. Including the extrapolated number of low-velocity-offset AGNs, as described in Section 2.4, this limit can reach 3%. Our merger fraction can include minor and major mergers, but because we cannot determine the mass ratios of the progenitor galaxies, we cannot be more specific about the mass range probed.

An estimate of the galaxy merger rate depends on both the timescale over which two SMBHs merge and the fraction of SMBHs that are visible as AGNs. Recall that two SMBHs in a merger spend  $t_{\text{combine}} \sim 100$  Myr at separations  $\gtrsim 1$  kpc. At separations  $\lesssim 1$  kpc, the SMBHs quickly sink to the bottom of the galaxy’s potential well due to dynamical friction and as a close binary can no longer be kinematically distinguished because their separation is smaller than the size of the [O III] emitting region. The fraction of SMBHs that power AGNs is  $f_{\text{lum}} \sim 10\%$  (Montero-Dorta et al. 2009), roughly consis-

tent with our measured fraction of red galaxies hosting AGNs (5%) and the fraction of dual AGNs in our sample of offset and dual AGNs (6%).

We include the expected number of offset and dual AGNs at low velocity differences to estimate the merger rate from our data. Correcting the parent sample of 1881 red galaxies by the fraction for which we can determine good absorption redshifts (95%; the rest are removed because the continuum signal-to-noise ratio is too low), we convert our estimate of 40 – 55 offset and dual AGNs into a galaxy merger fraction of 22 – 31% ( $10\% / f_{\text{lum}}$ ), or a galaxy merger rate of 2.2 – 3.1 mergers  $\text{Gyr}^{-1}$  ( $100 \text{ Myr} / t_{\text{combine}}$ ) ( $10\% / f_{\text{lum}}$ ) for DEEP2 red galaxies at  $0.34 < z < 0.82$ . Again, this merger rate can include both minor and major mergers.

The merger fraction of all galaxies is generally parameterized to evolve as  $(1+z)^n$ , where measurements of the exponent  $n$  range from 0 – 4 (e.g., Yee & Ellingson 1995; Woods et al. 1995; Patton et al. 1997). If the red galaxy merger fraction evolves significantly, we would expect a higher merger fraction for our sample than for a local sample. However, large uncertainties in the merger fraction evolution with redshift prevent us from making any direct comparisons.

A rough comparison, however, can be made between our merger fraction and other galaxy merger fractions derived observationally and semianalytically. van Dokkum (2005) found that 35% of early-type galaxies at  $0.05 < z < 0.2$  exhibit morphological signs of a recent merger, such as tidal tails and asymmetries in surface brightness. In addition, counts of close dynamical pairs of galaxies suggest that 24% of present day red galaxies have experienced gas-poor mergers with luminosity ratios between 1:4 and 4:1 since  $z \sim 1$  (Lin et al. 2008). Finally, semianalytic models of gas-poor major mergers suggest that  $\sim 5\%$  of  $M_B \lesssim -20$  galaxies at  $0.1 < z < 1.1$  have had a major merger in the past 1 Gyr (Bell et al. 2006).

Our red galaxy merger fraction of  $\sim 30\%$  is roughly consistent with galaxy merger fractions estimated from galaxy morphologies and close pairs of galaxies. This agreement is further evidence that the AGN velocity offsets we measure are the result of inspiralling SMBHs in galaxy mergers and not AGN outflows or gas kinematics (see Section 3).

Our merger fraction is much higher than the  $\sim 5\%$  merger fraction derived by semianalytic models, but this difference can be explained by differences in the merger mass ratios. The merger fraction from semianalytics considers only major mergers (mass ratios of 1:1 to 4:1), while our technique is sensitive to much higher mass ratios, provided that the less massive progenitor galaxy hosts a SMBH that can power an AGN. Significant differences in the methods and assumptions of different observational and theoretical approaches – especially the timescales involved – prevent a more direct comparison between merger fractions.

## 5. CONCLUSIONS

We have searched the DEEP2 Galaxy Redshift Survey for AGNs with velocities significantly different from the mean of the host galaxy’s stars, and have identified 30 objects with one set of offset AGN-fueled emission lines (“offset AGNs”) and two objects with two spatially resolved sets of AGN emission lines (“dual AGNs”). Al-

though a conspiracy between dust and gas kinematics or outflows could cause [O III] velocity offsets like those observed in our sample, our entire sample is unlikely to be the result of such effects unless the population of AGNs at our redshift range  $0.34 < z < 0.82$  is qualitatively different from the well-studied local population. Rather, the more plausible interpretation of our sample is that they are the results of recent galaxy mergers, during which two SMBHs spiral to the remnant's center at velocities different from the mean of the host galaxy's stars. If one or both of the SMBHs power AGNs, they will appear in our sample. Based on this interpretation, our main results are as follows.

1. We present the first systematic search for inspiralling SMBHs in galaxy mergers, from which we identify 32 such objects: 30 offset AGNs and two dual AGNs. Our technique of selecting these objects by the velocity offsets of their AGN emission lines relative to the host galaxy's stars is a new and powerful way of identifying galaxies that are the products of recent mergers.

2. About half of the red galaxies hosting AGNs are also merger remnants, which signals a strong correlation between AGN activity and mergers of gas-poor galaxies.

3. For DEEP2 red galaxies at  $0.34 < z < 0.82$ , the merger fraction is  $\sim 30\%$  ( $10\% / f_{\text{lum}}$ ), with a hard lower limit of  $2\%$ , and the merger rate is  $\sim 3$  mergers  $\text{Gyr}^{-1}$  ( $100 \text{ Myr} / t_{\text{combine}}$ ) ( $10\% / f_{\text{lum}}$ ). This merger rate can include both minor and major mergers. Our merger fraction is in agreement with merger fractions derived through other observational techniques, lending

additional support to our interpretation that the AGN velocity offsets we measure are the result of inspiralling SMBHs in galaxy mergers and not other physical mechanisms.

While other observational methods of determining the galaxy merger rate include no information about the state of the SMBHs in the merger, our new method is unique in that it selects merger-remnant galaxies with inspiralling SMBHs. Merging SMBHs are predicted to produce gravity waves, and although our offset and dual AGNs do not probe SMBH separations on the small scales where gravitational radiation is significant, our measurements also constrain the rate of SMBH mergers of interest to proposed gravitational wave detectors such as LISA (Bender et al. 1998).

J.M.C. acknowledges support from NSF grant AST-0507428. B.F.G. was supported by the U.S. Department of Energy under contract number DE-AC3-76SF00515. M.C.C. acknowledges support by NASA through the Spitzer Space Telescope Fellowship program. A.L.C. is supported by NASA through Hubble Fellowship grants HF-01182.01-A, awarded by the Space Telescope Science Institute. This work was also supported in part by NSF grants AST-0071048, AST-0071198, and AST-0507483. B.F.G. thanks the Aspen Center for Physics for its hospitality, and we also thank Jay Dunn and Mike Crenshaw for illuminating conversations.

#### REFERENCES

- Baldwin, J. A., Phillips, M. M., & Terlevich, R. 1981, *PASP*, 93, 5  
 Barth, A. J., Bentz, M. C., Greene, J. E., & Ho, L. C. 2008, *ApJ*, 683, L119  
 Begelman, M. C., Blandford, R. D., & Rees, M. J. 1980, *Nature*, 287, 307  
 Bekenstein, J. D. 1973, *ApJ*, 183, 657  
 Bell, E. F., et al. 2006, *ApJ*, 640, 241  
 Bender, P., et al. 1998, *LISA Pre-Phase: A Report*, 2nd ed.  
 Bogdanović, T., Eracleous, M., & Sigurdsson, S. 2009, *ApJ*, 697, 288  
 Bonning, E. W., Shields, G. A., & Salviander, S. 2007, *ApJ*, 666, L13  
 Bruzual, G., & Charlot, S. 2003, *MNRAS*, 344, 1000  
 Bundy, K., Ellis, R. S., & Conselice, C. J. 2005, *ApJ*, 625, 621  
 Croton, D. J., et al. 2006, *MNRAS*, 365, 11  
 Das, V., Crenshaw, D. M., Kraemer, S. B., & Deo, R. P. 2006, *AJ*, 132, 620  
 Das, V., et al. 2005, *AJ*, 130, 945  
 Davies, R. I., Mueller Sánchez, F., Genzel, R., Tacconi, L. J., Hicks, E. K. S., Friedrich, S., & Sternberg, A. 2007, *ApJ*, 671, 1388  
 Davis, M., et al. 2007, *ApJ*, 660, L1  
 De Propris, R., Conselice, C. J., Liske, J., Driver, S. P., Patton, D. R., Graham, A. W., & Allen, P. D. 2007, *ApJ*, 666, 212  
 Dotti, M., Montuori, C., Decarli, R., Volonteri, M., Colpi, M., & Haardt, F. 2008, *ArXiv e-prints*  
 Eracleous, M., & Halpern, J. P. 2003, *ApJ*, 599, 886  
 Eracleous, M., Halpern, J. P., Gilbert, A. M., Newman, J. A., & Filippenko, A. V. 1997, *ApJ*, 490, 216  
 Ferrarese, L., & Merritt, D. 2000, *ApJ*, 539, L9  
 Gaskell, C. M. 1984, *New York Academy Sciences Annals*, 422, 349  
 Gaskell, C. M. 1988, in *Active Galactic Nuclei*, ed. H. R. Miller & P. J. Wiita, 61  
 Gaskell, C. M. 1996, in *Lecture Notes in Physics*, Berlin Springer Verlag, Vol. 471, *Jets from Stars and Galactic Nuclei*, ed. W. Kundt, 165  
 Gerke, B. F., et al. 2007, *ApJ*, 660, L23  
 Gerssen, J., Wilman, D. J., Christensen, L., Bower, R. G., & Wild, V. 2009, *MNRAS*, 393, L45  
 Greene, J. E., & Ho, L. C. 2005, *ApJ*, 627, 721  
 Guyon, O., Sanders, D. B., & Stockton, A. 2006, *ApJS*, 166, 89  
 Hopkins, P. F., Bundy, K., Hernquist, L., & Ellis, R. S. 2007, *ApJ*, 659, 976  
 Kauffmann, G., et al. 2003, *MNRAS*, 346, 1055  
 Kewley, L. J., Groves, B., Kauffmann, G., & Heckman, T. 2006, *MNRAS*, 372, 961  
 Kitzbichler, M. G., & White, S. D. M. 2008, *MNRAS*, 391, 1489  
 Komossa, S., Xu, D., Zhou, H., Storchi-Bergmann, T., & Binette, L. 2008a, *ApJ*, 680, 926  
 Komossa, S., Zhou, H., & Lu, H. 2008b, *ApJ*, 678, L81  
 Kormendy, J., & Richstone, D. 1995, *ARA&A*, 33, 581  
 Lin, L., et al. 2008, *ApJ*, 681, 232  
 Loeb, A. 2007, *Physical Review Letters*, 99, 041103  
 Lotz, J. M., et al. 2008, *ApJ*, 672, 177  
 Marble, A. R., Hines, D. C., Schmidt, G. D., Smith, P. S., Surace, J. A., Armus, L., Cutri, R. M., & Nelson, B. O. 2003, *ApJ*, 590, 707  
 Merritt, D., Milosavljević, M., Favata, M., Hughes, S. A., & Holz, D. E. 2004, *ApJ*, 607, L9  
 Merritt, D., Storchi-Bergmann, T., Robinson, A., Batcheldor, D., Axon, D., & Cid Fernandes, R. 2006, *MNRAS*, 367, 1746  
 Milosavljević, M., & Merritt, D. 2001, *ApJ*, 563, 34  
 Montero-Dorta, A. D., et al. 2009, *MNRAS*, 392, 125  
 Nelson, C. H., & Whittle, M. 1995, *ApJS*, 99, 67  
 —. 1996, *ApJ*, 465, 96  
 Patton, D. R., Pritchet, C. J., Yee, H. K. C., Ellingson, E., & Carlberg, R. G. 1997, *ApJ*, 475, 29  
 Peres, A. 1962, *Physical Review*, 128, 2471  
 Ruiz, J. R., Crenshaw, D. M., Kraemer, S. B., Bower, G. A., Gull, T. R., Hutchings, J. B., Kaiser, M. E., & Weistrop, D. 2005, *AJ*, 129, 73  
 Shields, G. A., Bonning, E. W., & Salviander, S. 2009, *ApJ*, 696, 1367  
 Springel, V., Di Matteo, T., & Hernquist, L. 2005a, *ApJ*, 620, L79  
 —. 2005b, *MNRAS*, 361, 776  
 Toomre, A., & Toomre, J. 1972, *ApJ*, 178, 623  
 Urrutia, T., Lacy, M., & Becker, R. H. 2008, *ApJ*, 674, 80  
 van Dokkum, P. G. 2005, *AJ*, 130, 2647  
 Veilleux, S., Shopbell, P. L., & Miller, S. T. 2001, *AJ*, 121, 198  
 Vrtilik, J. M., & Carleton, N. P. 1985, *ApJ*, 294, 106  
 Wetzell, A. R., Schulz, A. E., Holz, D. E., & Warren, M. S. 2008, *ApJ*, 683, 1  
 Willmer, C. N. A., et al. 2006, *ApJ*, 647, 853  
 Woods, D., Fahlan, G. G., & Richer, H. B. 1995, *ApJ*, 454, 32  
 Yan, R., Newman, J. A., Faber, S. M., Konidaris, N., Koo, D., & Davis, M. 2006, *ApJ*, 648, 281  
 Yee, H. K. C., & Ellingson, E. 1995, *ApJ*, 445, 37

Zamanov, R., Marziani, P., Sulentic, J. W., Calvani, M., Dultzin-Hacyan, D., & Bachev, R. 2002, *ApJ*, 576, L9